IET Image Processing

Research Article

IET Journals
The Institution of Engineering and Technology

Classification of malignant melanoma and benign skin lesions: implementation of automatic ABCD rule

ISSN 1751-9659
Received on 29th June 2015
Revised on 7th December 2015
Accepted on 17th January 2016
doi: 10.1049/iet-ipr.2015.0385
www.ietdl.org

Reda Kasmi ✉, *Karim Mokrani*

LTII Laboratory University of Bejaia-Algeria, Faculty of Technology, University of Bejaia, Bejaia, Algeria
✉ *E-mail: rdkasmi@gmail.com*

Abstract: The ABCD (asymmetry, border irregularity, colour and dermoscopic structure) rule of dermoscopy is a scoring method used by dermatologists to quantify dermoscopy findings and effectively separate melanoma from benign lesions. Automatic detection of the ABCD features and separation of benign lesions from melanoma could enable earlier detection of melanoma. In this study, automatic ABCD scoring of dermoscopy lesions is implemented. Pre-processing enables automatic detection of hair using Gabor filters and lesion boundaries using geodesic active contours. Algorithms are implemented to extract the characteristics of ABCD attributes. Methods used here combine existing methods with novel methods to detect colour asymmetry and dermoscopic structures. To classify lesions as melanoma or benign nevus, the total dermoscopy score is calculated. The experimental results, using 200 dermoscopic images, where 80 are malignant melanomas and 120 benign lesions, show that the algorithm achieves 91.25% sensitivity of 91.25 and 95.83% specificity. This is comparable to the 92.8% sensitivity and 90.3% specificity reported for human implementation of the ABCD rule. The experimental results show that the extracted features can be used to build a promising classifier for melanoma detection.

1 Introduction

The incidence of melanoma has been increasing for many decades. Worldwide, in 2010, 49,100 deaths were attributed to melanoma [1, 2]. The most effective treatment is early surgical excision. Excision at the earliest in-situ stage of melanoma results in no change in life expectancy [3]. Early detection could be facilitated by automatic lesion analysis.

Several approaches have been proposed to differentiate benign melanocytic lesions from malignant melanoma. Stolz *et al.* [4] and Nachbar *et al.* [5] developed the ABCD (asymmetry, border irregularity, colour and dermoscopic structure) rule of dermoscopy to characterise geometrical and structural lesion properties. The seven-point checklist for melanoma is based on seven characteristics comprised of three major and four minor criteria [6]. The three-point checklist [7] is useful, even by novices, for identifying melanoma and basal cell carcinoma based on three criteria. The CASH algorithm [8] rely on four characteristics, i.e. the number of existing colours, the lesion disorder (architecture), the asymmetry and the lesion homogeneity. Menzie *et al.* [9] counts negative and positive features. Pehamberger *et al.* [10], using pattern analysis, considers 11 structures and 7 colours along with their localisation and distribution within the lesion.

Skin imaging technology has improved in recent years, encouraging researchers to develop a non-invasive computer-aided diagnosis (CAD) for melanoma detection based on lesion's features. Garnavi *et al.* [11] used border and wavelet based texture methods for computer-aided melanoma diagnosis. Patwardhan *et al.* [12] used wavelet tree structures to distinguish melanoma from dysplastic nevus using the mean energy ratios. Ramezani *et al.* [13] proposed a melanoma recognition system using an support vector machine (SVM) classifier; the features detected are based on asymmetry, border irregularity, colour variation, diameter and texture of the lesion. Celebi *et al.* [14] combines the detection of blue-white veil structure with geometrical properties of the lesion: fractal dimension, asymmetry index, ellipticity and circularity. Di Leo *et al.* [15] developed an algorithm on epiluminescence microscopy data, to detect five of the seven features of the seven-point algorithm: blue-white veil, atypical pigment network, irregular streaks, irregular pigmentation and regression structures. Burroni *et al.* [16] used geometrical, colour and texture properties with a *K*-nearest neighbourhood and linear discriminant classifiers. Ferris *et al.* [17] used 54 features based on geometrical, colour and texture properties to build a decision forest classifier.

The ABCD rule is widely used by dermatologists. The acronyms for this method are

Asymmetry A: It evaluates asymmetry; two orthogonal axes bisect the lesion. For both axes, asymmetry is assessed regarding shape, colours and/or dermoscopic structures. A score of two is given if there is asymmetry along both axis, it is scored one if there is asymmetry along one axis, and zero otherwise.
Border B: The lesion is divided into eight octants (slices). For each slice, an irregular periphery receives a score of one, it is scored zero if it is regular. Therefore, the highest border score is eight, and the minimum score is zero.
Colour C: We look for the occurrence of the six colours (white, red, light brown, dark brown, blue-grey and black). The score is incremented by one for each existing colour.
Dermoscopic structures D: This evaluates the presence of the five different structures (network, structureless areas, branched streaks, dots and globules). The presence of each structure is scored one; therefore, the structure score ranges from 0 to 5.

To classify the lesion, the total dermoscopic score (TDS) (1) is computed. A low score means that the lesion is benign (TDS < 4.75), a middle score can be interpreted as a suspicious case (4.75 < TDS < 5.45) and a high score means that the lesion is more likely to be a malignant melanoma (TDS > 5.45)

$$\mathrm{TDS} = A * 1.3 + B * 0.1 + C * 0.5 + D * 0.5 \quad (1)$$

Digital ABCD rule systems have recently been implemented; Piccolo *et al.* [18] reported a digital ABCD rule based on shape asymmetry, rather than colour asymmetry. Their border '*B*' score

was based on the count of octants with a sharp border cutoff, as in the original clinical ABCD paper. The different structures are detected using various digital filters and classified using morphological analysis. For Smaoui and Bessassi [19], Ramteke and Jain [20] and Jaworek-Korjakowska [21], the *D* attribute is related to the diameter of the lesion. Any lesion with diameter >6 mm will have a *D* score equal to 5.

We report here a CADsystem for dermoscopic images analysis based on the ABCD rule. Unlike Piccolo's approach, the '*A*' score is based on shape, colour and luminance asymmetry. The *D* attribute relies, not only on network and blue-white veil structures, but also on lesion geometrical properties. These choices allow a better discrimination between melanoma and benign lesions.

The proposed algorithm consists of four main steps: (i) pre-processing to remove artefacts, such as hair, and to reduce the bubble intensity in the image; (ii) lesion contour detection; (iii) feature extraction and (iv) classification of the lesion.

2 Pre-processing

Artefacts such as bubbles and hair represent noise; it is necessary to remove them before any feature extraction for an accurate diagnosis [22].

2.1 Median filter

Bubbles that may appear on the lesion affect the measure of colour and luminosity asymmetry. An 11×11 median filters is used to reduce the impact of bubbles (Fig. 1); thin hair is removed as well [23].

The size of the filter (11×11) was determined empirically, and the choice is guided by two goals: reduction of bubbles intensity and prevention of fuzzy edges. Tests with different filter size show that 11×11 is optimal.

2.2 Hair detection

First, hair is segmented roughly using a set of three real Gabor filters with different frequencies and orientations (2)–(4). The convolution of the three Gabor kernels with the normalised inverse value plane (V) of the hue, saturation, value (HSV) colour system produce a high response for hair [24–26].

Table 1 shows the Gabor kernel parameters. The three resulting images are binarised using an empirically fixed threshold ($T = 0.7$). Small objects are removed from the hair mask, using mathematical morphology and object properties (area, eccentricity and object length). The final mask is the result of overlaying the three masks by a logical OR operator. Finally, the hair is repaired by linear interpolation [27]. On the same image set, with manually drawn hair masks, the sensitivity of the algorithm is 68.57% while DullRazor [28] achieves 54.45% [29]

Table 1 Parameters of the three Gabor kernels

	Kernel 1	Kernel 2	Kernel 3
σ_u	2	2	2
σ_v	6	4	6
f_0	0.03	0.06	0.07
θ	0°	45°	90°

$$G_\theta(U, V) = \exp\left(-1\left[\frac{U'^2}{\sigma_u^2} + \frac{V'^2}{\sigma_v^2}\right]\right)\cos(2\pi f_0 U) \tag{2}$$

where

$$U' = U\cos(\theta) + V\sin(\theta) \tag{3}$$

$$V' = -U\cos(\theta) + V\sin(\theta) \tag{4}$$

The entire hair-removal process is shown in the diagram in Fig. 2. The results of the hair removal algorithm are shown in Fig. 3.

3 Contour detection

Among the contour detection techniques [30–32], the geodesic active contour (GAC) method provides an effective framework for image segmentation. It has been commonly used in biomedical image, due to its adaptability to the topological changes of the object shape [33]. In this work, the GAC is applied on the first *Karhunen–Loève transform* (KLT) component, which is optimal in the sense that it contains the maximum variance. Variations primarily occur at boundaries between lesions and surrounding skin.

To find the initial GAC contour, the first component of the KLT transform is smoothed using a 20×20 median filter. The resulting component is binarised using Otsu's algorithm [34]. The Otsu threshold is reduced by 5 as in [32]. Using the binarised image, the largest and closest object to the centre is chosen as the initial contour.

Equation (5) shows the primary GAC equation, based on curve evolution theory. Equation (6) makes the evolution of the contour stops at the lesion's boundary [35, 36]

$$\frac{\partial C(t)}{\partial t} = (g(I)k - < \nabla g(I), \boldsymbol{N} >)\boldsymbol{N} \tag{5}$$

$$g(I) = \frac{1}{1 + (\nabla I)^2} \tag{6}$$

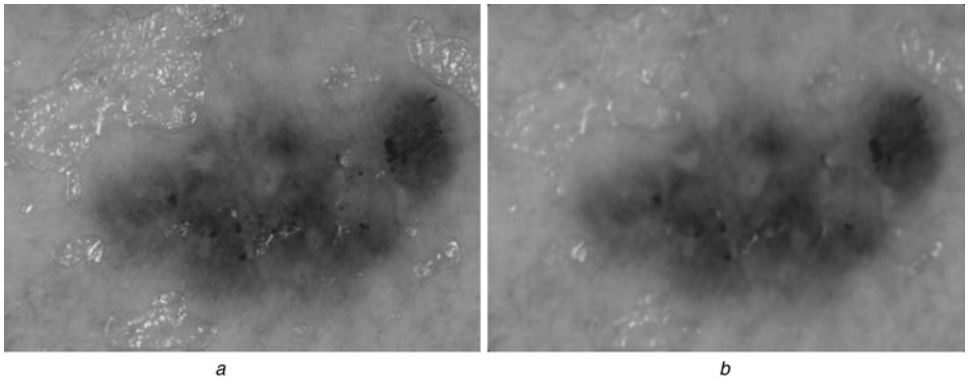

a b

Fig. 1 *Median filter influence on the bubbles*

a Original image
b Filtered image

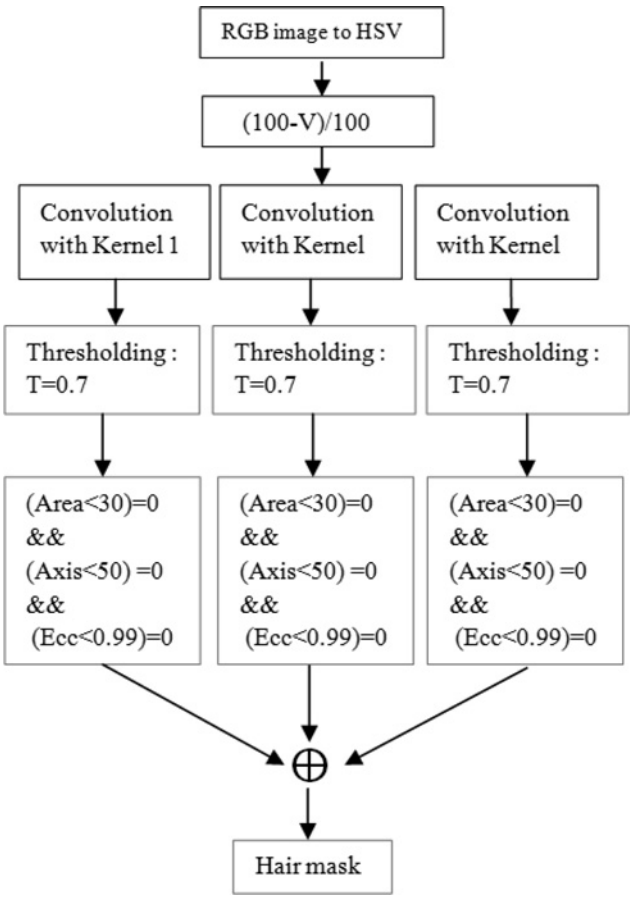

Fig. 2 *Hair removal algorithm*

where ∇I is the gradient of the greyscale image, g is the decreasing function, k is the curvature and $\boldsymbol{N}$ is the unit vector in the normal direction (Fig. 4)

On a data set of 100 images, with contours drawn manually by an expert, the algorithm yields an error of 6.7%, while the average contour made by three dermatologists yields an error of 7.4% [37].

4 Features extraction

Melanomas have a propensity to grow chaotically and incoherently. Therefore, lesions have asymmetric shapes, colours, structures and uneven borders. The irregular variations should characterise all features including asymmetry, border, colour and the structures within the lesion.

4.1 Asymmetry

Asymmetry measures include colour, brightness and lesion shape. To find the axes of symmetry, the horizontal and vertical axes crossing at the centre of gravity of the lesion are drawn. The first principal axis of symmetry $I(\varphi)$ crosses the centre of gravity with a slant angle φ to the horizontal axis [38, 39]

$$I(\varphi) = \sum_{(i,j)\in L} D_{\varphi}^{2}(i,j) \tag{7}$$

$$I(\varphi) = \sum_{(i,j)\in L} \left[-i\sin(\varphi) + j\cos(\varphi)\right]^{2} \tag{8}$$

$D_{\varphi}(i,j)$ is the distance between the current pixel and the horizontal line.

φ is given by

$$\frac{\partial I(\varphi)}{\partial(\varphi)} = 0 \quad \text{then} \quad \varphi_0 = 0.5\tan^{-1}\left[\frac{2m_{11}}{m_{20} - m_{02}}\right] \tag{9}$$

where m_{11} is the standard product moment and (m_{20}, m_{02}) is the second-order moments with respect to the horizontal and vertical axes.

The final mask shown in Fig. 5*c* is obtained by rotating Fig. 5*b* by $-\varphi$.

4.1.1 Colour asymmetry: The image is subdivided into blocks of 20×20 pixels. We select only those who have at least 75% of their area inside the lesion. The colour average of each selected block is computed (Fig. 6).

We measure the colour distance between two symmetrical blocks along the two principal axes.

The image is converted to the L^*a^*b colour system, because it is considered to be perceptually uniform, i.e. the Euclidean distance between two colours in La^*b^* space approximates the difference perceived by humans [40, 41]

$$\Delta E = \sqrt{(L_{b1} - L_{b2})^2 + (a_{b1} - a_{b2})^2 + (b_{b1} - b_{b2})^2} \tag{10}$$

where ΔE is the Euclidean distance, (L_{b1}, a_{b1}, b_{b1}) are the components of the first block and (L_{b2}, a_{b2}, b_{b2}) are the components of the opposite block.

The JND (just noticeable distance) is used as a threshold to differentiate colours. It is the minimal colour variation noticeable by the human eye [41, 42]. The JND is defined as in Table 2.

Although Sharma and Bala [42] cites a smaller JND $\sim$ 22.3, we allow a looser JND threshold of 6, to accommodate biologic variability. Along any axis, for any pair of blocks, if JND ≤ 6, the block pair is said to be colour symmetric.

In the example shown in Fig. 6, along the horizontal axis, the number of blocks with JND ≤ 6 is 32 and the number of blocks with JND > 6 is 11 (Fig. 7*a*). Along the vertical axis, the number of blocks with JND ≤ 6 is 39 and the number of blocks with JND > 6 is 5 (Fig. 7*b*).

Along any axis, if the number of blocks that are colour symmetric is greater than the number of colour asymmetrical blocks, the image is said to be colour symmetric along that axis.

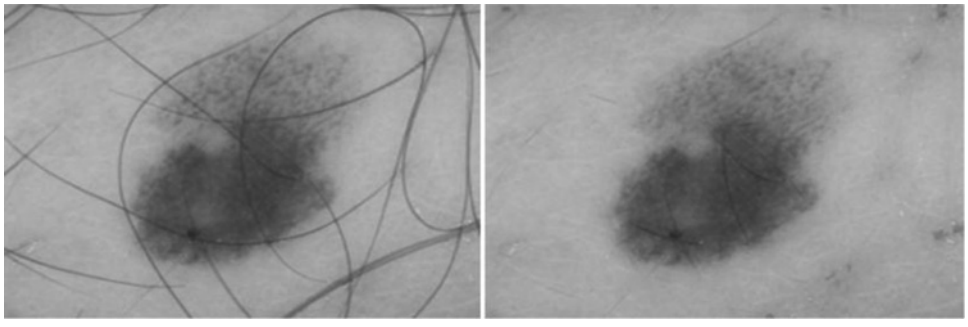

Fig. 3 *Hair removal algorithm results*

IET Image Process., 2016, Vol. 10, Iss. 6, pp. 448–455

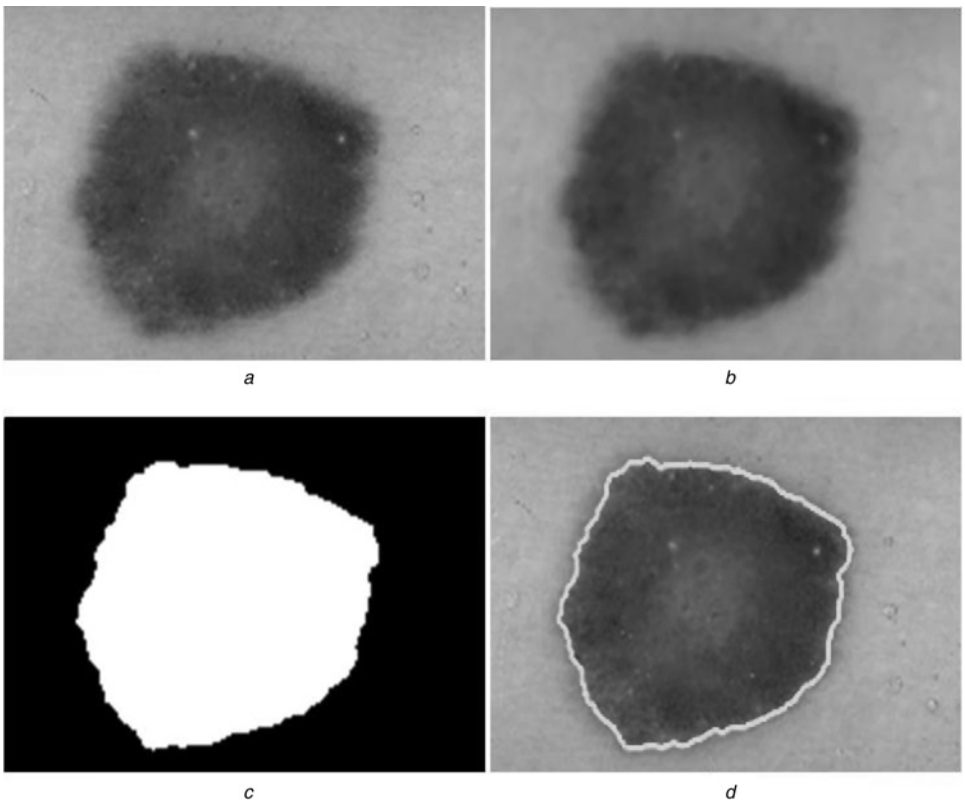

Fig. 4 *Contour detection*

a Original image
b First KLT component
c Mask
d Contour

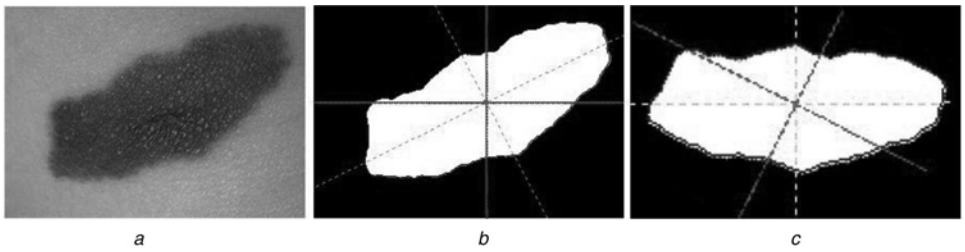

Fig. 5 *Preparing the image for asymmetry measurement*

a Original image
b, *c* Final mask with axes of symmetry (dotted lines)

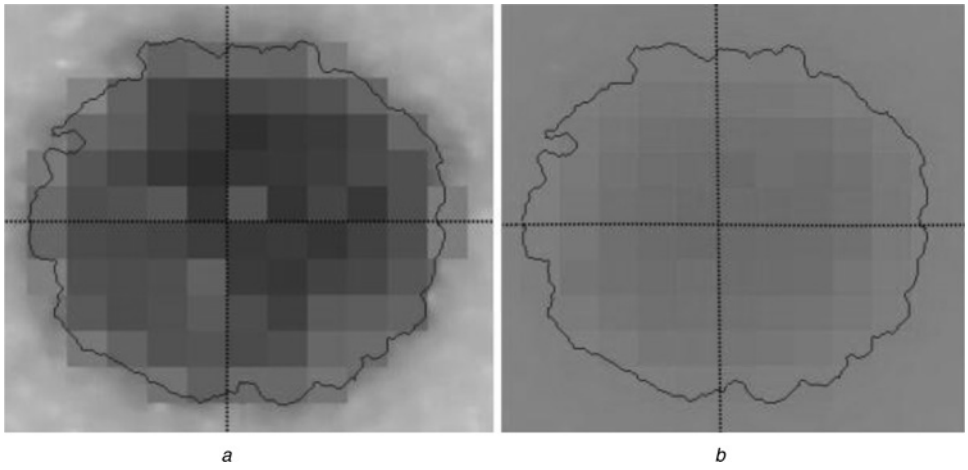

Fig. 6 *Lesion blocks*

a Image in RGB
b Image in *l***a***b*

Table 2 Limit of perceptible colour distance

$\Delta E^*_{L^*a^*b^*}$	Effect
*<3	not perceptible
3<*< = 6	barely perceptible but acceptable
*>6	perceptible

4.1.2 Brightness asymmetry: The brightness asymmetry is measured by the difference between the average luminance of two opposite halves of the lesion along one symmetry axis [43]. The threshold is set to 3% of the total average luminance of the lesion. For one axis, if the brightness asymmetry measure is less than the threshold, the image is said to be brightness symmetric along that axis.

4.1.3 Shape asymmetry: Shape asymmetry along one axis is measured by the difference between the lesion areas above and below that axis. Both axes, horizontal and vertical, are considered. The shape asymmetry threshold is set to 2% of the lesion area.

For a given axis, the lesion is said to be symmetric if it is simultaneously colour, brightness and shape symmetric along that axis. The asymmetry score is set to zero if the lesion is symmetric along both axes, set to one if it is symmetric along only one axis and set to two otherwise.

4.2 Border

The lesion is divided into eight equal octants (slices) (Fig. 8). Then, the sub-contour of each slice is approximated by a third-order spline function (10)

$$p(x) = p_1x^3 + p_2x^2 + p_3x^1 + p_4 \tag{11}$$

Finally, the fitting error is computed by (12). If the error exceeds $0.05 \times$ length of y (sub-contour), the sub-contour is said to be irregular

$$E = \sqrt{\frac{\left(\sum_{i=1}^{\text{length}(y)} |p(i) - y(i)|\right)^2}{\text{length}(y)}} \tag{12}$$

where y is the sub-contour.

For an irregular sub-contour the score is set to one. For a lesion, the total score goes from zero to eight.

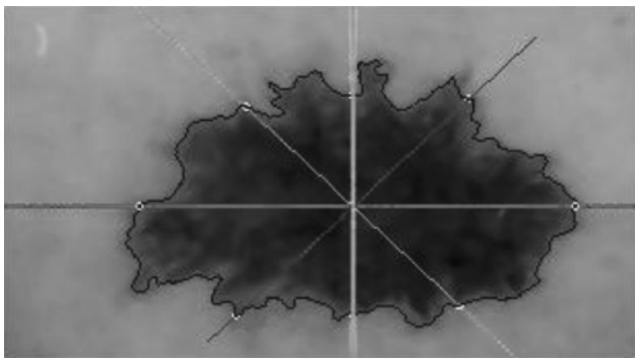

Fig. 8 *Image divided into eight octants (slices), each subtending 45°*

4.3 Colour

According to the ABCD rule, lesions with one of the six suspicious colours (white, black, red, light-brown, dark-brown and blue-grey) are likely to be melanomas. These six colours are represented in red, green, blue (RGB). These values are obtained from a manually segmented lesion (Fig. 9).

The normalised Euclidean distances between each pixel of the lesion and the six suspicious colours are measured. A pixel belongs to a given colour if the distance is less than a fixed threshold T. T is set to 0.4, a distance that is approximately half the distance between the two extremes colours, that are white and black: 0.7783 [44].

In a lesion, a colour suspicious for melanoma occurs if the number of pixels belonging to that colour exceeds by 5% of the total number of pixels of the lesion. In a lesion, more than one suspicious colour can occur.

Colour	RGB Values
White	[197 188 217]
Black	[41 31 30]
Red	[118 21 17]
Light-brown	[163 82 16]
Dark-brown	[135 44 05]
Blue-gray	[113 108 139]

Fig. 9 *Six melanoma colours, in RGB value*

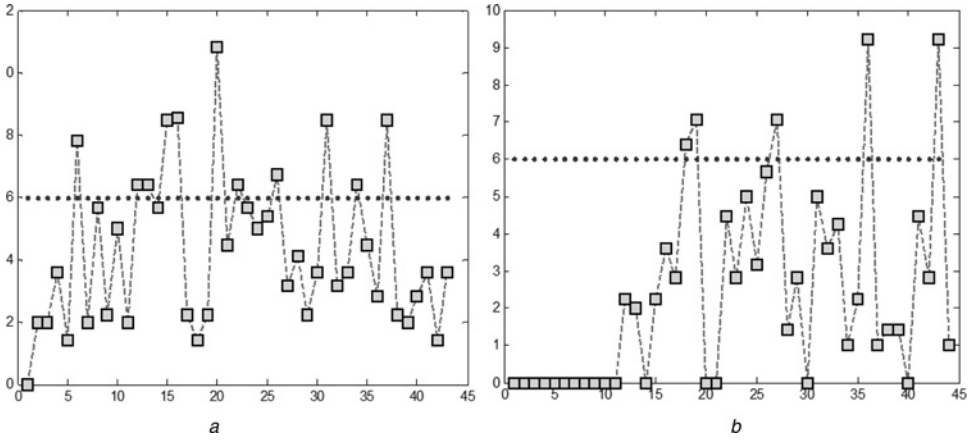

Fig. 7 *Colour distances for symmetric block pairs*

a Along the horizontal axis
b Along vertical axis

IET Image Process., 2016, Vol. 10, Iss. 6, pp. 448–455

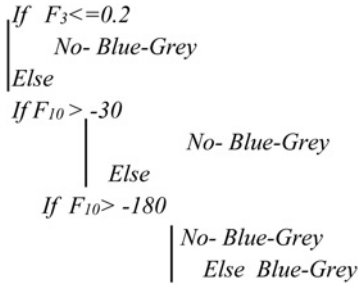

Fig. 10 *Threshold which fit to our dataset*

4.4 Different structures

In this work, we detect two structures: pigment network as in [22] and blue-white veils as in [14]. To evaluate the D attribute, scored 0–5 points, geometrical properties of the lesion are measured and scored 0–3 points. Finally, the D is measured as

$D =$ (score of two structures)

$+$ (result of the classifier based on the geometrical properties)

4.4.1 Pigment network: Anantha *et al.* [22] developed an algorithm to detect pigment network. The lesion is divided into sub-blocks of size 20×20. For each block we look for pigment network using the L and E Laws masks. The algorithm is as follows

$$L = \begin{bmatrix} 1 & 2 & 1 \end{bmatrix}$$

$$E = \begin{bmatrix} -1 & 2 & -1 \end{bmatrix}$$

For each 20×20 block of greyscale image (I_{g20*20})

$$\mathrm{WL} = \mathrm{conv}\left(I_{g20*20}, L\right)$$

$$\mathrm{WL} = \frac{1}{40}\sum_{j=1}^{20}\sum_{i=1}^{20}\mathrm{WL}(i,j)^2 \tag{13}$$

$$\mathrm{WE} = \frac{1}{40}\sum_{j=1}^{20}\sum_{i=1}^{20}\mathrm{WE}(i,j)^2 \tag{14}$$

If WL > TL1 and WE > TL2

If $R >$ TL3 and $\dfrac{R+G}{2} >$ TL4

Pigment network

Else if
No pigment network
Else if
No pigment network

where TL1 = 90,000, TL2 = 90,000, TL3 = 45, TL4 = 55 and Con is the convolution.

4.4.2 Blue-white veil: Celebi *et al.* [14] developed an algorithm to detect blue-white veil using the chromaticity coordinates F_3 and F_{10}. These coordinates are defined as

$$F_3 = \frac{B_\mathrm{L}}{R_\mathrm{L} + G_\mathrm{L} + B_\mathrm{L}} \tag{15}$$

$$F_{10} = R_\mathrm{L} - R_\mathrm{s} \tag{16}$$

where (R_L, G_L, B_L) is the average lesion colour and R_s is the average red skin colour.

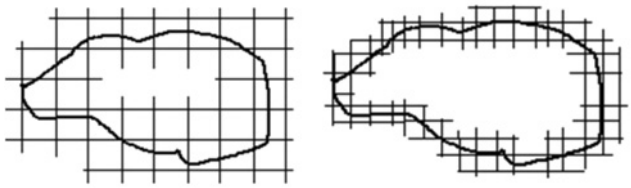

Fig. 11 *Fractal dimension box-counting method*

We used the same classification tree as in [14], but the threshold which fit to our dataset is shown in Fig. 10.

4.4.3 Geometrical properties: Four lesion shape features are measured: fractal dimension, asymmetry index, circularity and elasticity.

Fractal dimension fd*:* It is a multi-scale method that has been shown to possess a strong correlation with the natural impression of roughness for curved lines in human vision [45, 46]. The fd analysis evaluates contour irregularity [47, 48].

The image is divided into grids of size $r \times r$. $N(r)$ evaluates the contour length in the grid (Fig. 11).

The contour length L converges to its 'true value', as r decreases [45]

$$L = N(r)r \tag{17}$$

$$N(r) = \lambda r^{-\mathrm{fd}} \tag{18}$$

where λ is a scaling constant and fd is the characteristic of the coast line known as fractal dimension

$$\log\frac{1}{N(r)} = \mathrm{fd} \times \log(r) - \log(\lambda) \tag{19}$$

Asymmetry index: The shape of melanomas tends to be asymmetric

$$\mathrm{AI} = \frac{1}{2}\sum_{k=1}^{2}\frac{\Delta A_k}{A_\mathrm{L}} \tag{20}$$

where k is the major and minor axis, ΔA_k is the non-overlapping lesion areas along k and A_L is the lesion area.

Ellipticity and circularity: Melanomas tend to be more elliptic in shape contrary to benign lesions. Ellipticity is computed along the major axis as in [14]

$$S_1 = \begin{cases} 16\pi^2 A_1 & \text{if } A_1 \le \dfrac{1}{16\pi^2} \\ \dfrac{1}{16\pi^2 A_1} & \text{otherwise} \end{cases} \tag{21}$$

$$A_1 = \frac{u_{20}u_{02} - u_{11}^2}{u_{00}^4} \tag{22}$$

The circularity is defined as

$$S_2 = \frac{m_R}{\sigma_R} \tag{23}$$

where

$$m_R = \frac{1}{P}\sum_{k=1}^{P}(r_k, c_k) - (\bar{r}, \bar{c}) \tag{24}$$

$$\sigma_R = \left(\frac{1}{P}\sum_{k=1}^{P}\left((r_k, c_k) - (\bar{r}, \bar{c}) - m_R\right)^2\right)^{1/2} \tag{25}$$

The four lesion shape features are used to build the classifier as shown in Fig. 12.

```
If  S1>0.85&AI>0.4
|Score=3
  Elseif  S2< 0.85&AI>0.55
    Score=2
    |  Elseif  fd >1
    |    |  Score=2
    |    |    |  Else
    |    |    |  |  Score=0
```

Fig. 12 *Four lesion shape features that are used to build the classifier*

5 Materials

The image test set used in this paper consists of 200 digital contact non-polarised dermoscopic images obtained from the EDRA Interactive Atlas of Dermoscopy, where 80 are melanoma and 120 are benign [49]. Images are full colour 24-bit with typical resolutions of 712 × 454.

6 Results

The algorithm reaches an overall accuracy of 94.0%, achieving sensitivity and a specificity of 91.25% and 95.83, respectively, as shown in Table 4. Nachbar *et al.* [5], with a manual implementation of the ABCD rule, reported a sensitivity and a specificity of 92.80 and 90.30%, respectively. The results show that the extracted features are useful for a computer-assisted melanoma identification tool. However, the approach misclassified 12 lesions: seven melanomas and five benign cases. The results are summarised in Tables 3 and 4

$$\text{Specificity} = \frac{\text{TN}}{\text{TN} + \text{FP}} \tag{26}$$

$$\text{Sensitivity} = \frac{\text{TP}}{\text{TP} + \text{FN}} \tag{27}$$

$$\text{Accuracy} = (\text{TP} + \text{TN})/(\text{TP} + \text{FP} + \text{TN} + \text{FN}) \tag{28}$$

7 Discussion

We noticed two major problems that cause misclassification: bad contour detection and the inability to detect structures.

Fig. 13 represent a typical case where the colour of a part of the lesion is close to the healthy skin colour. The initial contour of the GAC cannot stop at the true boundary, since the stopping criteria

Table 3 Results of the proposed approach

	Classified as melanoma	Classified as benign
melanoma (80)	TP = 73 (91.25%)	FP = 7 (08.75%)
benign (120)	FN = 5 (04.16%)	TN = 115 (95.83%)

True positive (TP)
True negative (TN)
False positive (FP)
False negative (FN)

Table 4 Statistical results for the proposed approach

Sensitivity	Specificity	Positive predictive value	Negative predictive value
73/80 * 100% (91.25%)	115/120 * 100% (95.83%)	73/78 * 100% (93.59%)	115/122 * 100% (94.26%)

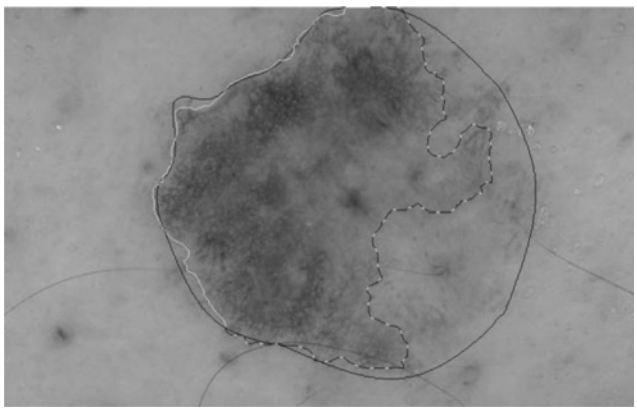

Fig. 13 *Segmentation: manual border (black), automatic border (white) and false boundary (dashed line)*

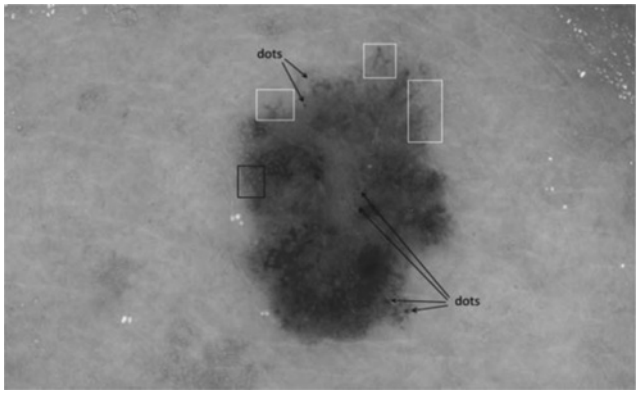

Fig. 14 *Melanoma classified as benign*

of the GAC relies on a high contrast gradient, found at the dashed line. To achieve a 'dermatologist-like boundary', which includes areas generally beyond high-gradient borders [50], constraints should be added in the stopping term in the GAC equation. It is anticipated that heavy filtering and better initial boundaries will accomplish inclusion of more areas despite high gradient at false 'inner boundaries' (dashed line in Fig. 13).

The automatic contour (white) is twisted compared with the manual contour (black). The values of the border irregularity '*B*', asymmetry '*A*' and geometrical properties used for '*D*' are affected. The corresponding scores for *A*, *B*, *C* and *D* are 2, 4, 2 and 3, respectively, instead of 1, 1, 2 and 1.

The computed TDS is then 5.5 instead of 2.8. The benign lesion is classified as melanoma since its TDS is higher than 4.75.

Fig. 14 shows a melanoma with an atypical pigment network (black box), irregular streaks (white box) and white structureless areas in the centre of the lesion.

The corresponding scores for *A*, *B*, *C* and D are 1, 3, 3 and 1, respectively, instead of 1, 3, 4 and 4. The computed TDS is 4.1 instead of 5.6. The melanoma is classified as benign since its TDS is lower than 4.75.

Moreover, the lack of manually segmented images with streaks, dots and globules structures annotated by an expert did not allow us to test our approach on these types of images.

Table 5 Comparison of different automatic ABCD rule implementation

	Images	Accuracy, %
Piccollo *et al.* [18]	165	78
Ramteke and Jain [20]	30	90
Smaoui and Bessassi [19]	40	92
proposed approach	200	94

IET Image Process., 2016, Vol. 10, Iss. 6, pp. 448–455

In summary, the automatic digital dermoscopy scoring systems reported to date, utilise analysis of features such as colour, size, location and texture. A comparison with the results of different automatic implementation of the ABCD rule is given in Table 5; however, the results should be taken with care since the reported studies use different image sets.

8 Conclusion

In this study, image processing techniques were used for an automatic ABCD rule implementation to discriminate malignant melanoma from benign lesions. We rely on a pre-processing step based on a median filter to remove artefacts (bubbles and thin hair). Thick hairs are detected using Gabor filters with different frequencies and orientations. Based on the hair mask, the image is repaired using linear interpolation. Lesions are segmented by a GAC. The values of A, B, C and D are estimated and the TDS is computed. Experiments on a set of 200 digital dermoscopic images, where 80 are melanomas and 120 are benign, achieve an overall accuracy of 94.0%. The experimental results show that the selected features are good candidates for an automatic melanoma detection algorithm. The proposed approach may represent a very useful tool for less experienced dermatologists and clinicians. To the best of our knowledge, compared with the existing automatic implementations of the ABCD rule, we achieve the highest accuracy, however, the results should be taken with care since the reported studies use different image sets. Future work could allow further improvement, primarily in the artefact removal steps and in structures detection.

9 References

1 Lozano, R., Naghavi, M., Foreman, K.: 'Global and regional mortality from 235 causes of death for 20 age groups in 1990 and 2010: a systematic analysis for the global burden of disease study 2010', *Lancet*, 2013, **380**, (9859), pp. 2095–2128

2 Godar, D.E.: 'Worldwide increasing incidences of cutaneous malignant melanoma', *J. Skin Cancer*, 2011, **2011**

3 Mocellin, S., Nitti, D.: 'Cutaneous melanoma in situ: translational evidence from a large population-based study', *Oncologist*, 2011, **16**, (6), pp. 896–903

4 Stolz, W., Riemann, A., Cognetta, A., *et al.*: 'ABCD rule of dermatoscopy-a new practical method for early recognition of malignant-melanoma', *Eur. J. Dermatol.*, 1994, **4**, (7), pp. 521–527

5 Nachbar, F., Stolz, W., Merkle, T., *et al.*: 'The ABCD rule of dermatoscopy: high prospective value in the diagnosis of doubtful melanocytic skin lesions', *J. Am. Acad. Dermatol.*, 1994, **30**, (4), pp. 551–559

6 Argenziano, G., Catricalà, C., Ardigo, *et al.*: 'Seven-point checklist of dermoscopy revisited', *Br. J. Dermatol.*, 2011, **164**, (4), pp. 785–790

7 Zalaudek, I., Argenziano, G., Soyer, H., *et al.*: 'Three-point checklist of dermoscopy: an open internet study', *Br. J. Dermatol.*, 2006, **154**, (3), pp. 431–437

8 Henning, J.S., Dusza, S.W., Wang, S.Q., *et al.*: 'The cash (colour, architecture, symmetry, and homogeneity) algorithm for dermoscopy', *J. Am. Acad. Dermatol.*, 2007, **56**, (1), pp. 45–52

9 Menzies, S.W., Crotty, K.A., Ingvar, C., *et al.*: 'An atlas of surface microscopy of pigmented skin lesions: dermoscopy' (McGraw-Hill Roseville, 2003)

10 Pehamberger, H., Steiner, A., Wolff, K.: 'In vivo epiluminescence microscopy of pigmented skin lesions. i. pattern analysis of pigmented skin lesions', *J. Am. Acad. Dermatol.*, 1987, **17**, (4), pp. 571–583

11 Garnavi, R., Aldeen, M., Bailey, J.: 'Computer-aided diagnosis of melanoma using border-and wavelet-based texture analysis', *IEEE Trans. Inf. Technol. Biomed.*, 2012, **16**, (6), pp. 1239–1252

12 Patwardhan, S.V., Dhawan, A.P., Relue, P.A.: 'Classification of melanoma using tree structured wavelet transforms', *Comput. Methods Programs Biomed.*, 2003, **72**, (3), pp. 223–239

13 Ramezani, M., Karimian, A., Moallem, P.: 'Automatic detection of malignant melanoma using macroscopic images', *J. Med. Signals Sens.*, 2014, **4**, (4), p. 281

14 Celebi, M.E., Iyatomi, H., Stoecker, W.V.: 'Automatic detection of blue-white veil and related structures in dermoscopy images', *Comput. Med. Imaging Graph*, 2008, **32**, (8), pp. 670–677

15 Di Leo, G., Paolillo, A., Sommella, P., *et al.*: 'Automatic diagnosis of melanoma: a software system based on the 7-point check-list'. 2010 43rd Hawaii Int. Conf. on System Sciences (HICSS), 2010

16 Burroni, M., Corona, R., Dell'Eva, G., *et al.*: 'Melanoma computer-aided diagnosis reliability and feasibility study', *Clin. Cancer Res.*, 2004, **10**, (6), pp. 1881–1886

17 Ferris, L.K., Harkes, J.A., Gilbert, B., *et al.*: 'Computer-aided classification of melanocytic lesions using dermoscopic images', *J. Am. Acad. Dermatol.*, 2015, **73**, (5), pp. 769–776

18 Piccolo, D., Crisman, G., Schoinas, S., *et al.*: 'Computer-automated ABCD versus dermatologists with different degrees of experience in dermoscopy', *Eur. J. Dermatol.*, 2014, **24**, (4), pp. 477–481

19 Smaoui, N., Bessassi, S.: 'A developed system for melanoma diagnosis', *Int. J. Comput. Vis. Signal Process.*, 2013, **3**, (1), pp. 10–17

20 Ramteke, N.S., Jain, S.V.: 'ABCD rule based automatic computer-aided skin cancer detection using Matlab®', *Int. J. Comput. Technol. Appl.*, 2013, **4**, (4), p. 691

21 Jaworek-Korjakowska, J.: Automatic detection of melanomas: an application based on the Abcd criteria', *Inf. Technol. Biomed.*, (Springer-Berlin, Heidelberg, 2012), pp. 67–76

22 Anantha, M., Moss, R.H., Stoecker, W.V.: 'Detection of pigment network in dermatoscopy images using texture analysis', *Comput. Med. Imaging Graph*, 2004, **28**, (5), pp. 225–234

23 Messadi, M., Bessaid, A., Taleb-Ahmed, A.: 'Extraction of specific parameters for skin tumour classification', *J. Med. Eng. Technol.*, 2009, **33**, (4), pp. 288–295

24 Van Deemter, J.H., du Buf, J.H.: 'Simultaneous detection of lines and edges using compound Gabor filters', *Int. J. Pattern Recognit. Artif. Intell.* , 2000, **14**, (06), pp. 757–777

25 Liu, Z.Q., Cai, J.H., Buse, R.: 'Handwriting recognition: soft computing and probabilistic approaches' (Springer, 2012)

26 Daugman, J.G.: 'Uncertainty relation for resolution in space, spatial frequency, and orientation optimized by two-dimensional visual cortical filters', *J. Opt. Soc. Am. A*, 1985, **2**, (7), pp. 1160–1169

27 Toossi, M.T.B., Pourreza, H.R., Zare, H., *et al.*: 'An effective hair removal algorithm for dermoscopy images', *Skin Res. Technol.*, 2013, **19**, (3), pp. 230–235

28 Lee, T., Ng, V., Gallagher, R., *et al.*: 'Dullrazor®: a software approach to hair removal from images', *Comput. Biol. Med.*, 1997, **27**, (6), pp. 533–543

29 Mokrani, K., Kasmi, R., Arour, M.: 'Technique d'élimination des poils pour les images dermoscopiques'. National Conf. on Electronics and New Technologies, 2015

30 Wang, H., Chen, X., Moss, R.H., *et al.*: 'Watershed segmentation of dermoscopy images using a watershed technique', *Skin Res. Technol.*, 2010, **16**, (3), pp. 378–384

31 Celebi, M.E., Iyatomi, H., Schaefer, G., *et al.*: 'Lesion border detection in dermoscopy images', *Comput. Med. Imaging Graph*, 2009, **33**, (2), pp. 148–153

32 Erkol, B., Moss, R.H., Joe Stanley, R., *et al.*: 'Automatic lesion boundary detection in dermoscopy images using gradient vector flow snakes', *Skin Res. Technol.*, 2005, **11**, (1), pp. 17–26

33 Lee, C.P.: 'Robust image segmentation using active contours: level set approaches'. PhD thesis, North Carolina State University, 2005

34 Otsu, N.: 'A threshold selection method from grey level histograms', *IEEE Trans. Syst. Man Cybern.*, 1979, **9**, pp. 62–66

35 Caselles, V., Kimmel, R., Sapiro, G.: 'Geodesic active contours', *Int. J. Comput. Vis.*, 1997, **22**, (1), pp. 61–79

36 Sethian, J.A.: 'Level set methods and fast marching methods', *J. Comput. Inf. Technol.*, 2003, **11**, (1), pp. 1–2

37 Kasmi, R., *et al.*: 'Biologically inspired skin lesion segmentation using a geodesic active contour technique,' *Skin Res. Technol.*, 2015, doi: 10.1111/srt.12252

38 Zagrouba, E., Barhoumi, W.: 'A prelimary approach for the automated recognition of malignant melanoma', *Image Anal. Stereol.*, 2004, **23**, pp. 121–135

39 Messadi, M., Bessaid, A., Taleb-Ahmed, A.: 'New characterization methodology for skin tumors classification', *J. Mech. Med. Biol.*, 2010, **10**, (03), pp. 467–477

40 Risson, V.: 'Application De La Morphologie Mathématique À L'analyse Des Conditions D'éclairage Des Images Couleur' (École Nationale Supérieure des Mines de Paris, 2001)

41 Farrugia, J.P.: 'Modèles De Vision Et Synthèse D'images' (Ecole Nationale Supérieure des Mines de Saint-Etienne; Université Jean Monnet-Saint-Etienne, 2002)

42 Sharma, G., Bala, R.: 'Digital colour imaging handbook' (CRC Press, 2002)

43 Seidenari, S., Pellacani, G., Grana, C.: 'Early detection of melanoma by image analysis', *Bioeng. Skin, Skin Imaging Anal.*, 2006, **31**, pp. 305–311

44 Grammatikopoulos, G., Hatzigaidas, A., Papastergiou, A., *et al.*: 'Automated malignant melanoma detection using Matlab'. Proc. Fifth Int. Conf. on Data Networks, Communications and Computers, Bucharest, Romania, 2006

45 Claridge, E., Hall, P., Keefe, M., *et al.*: 'Shape analysis for classification of malignant melanoma', *J. Biomed. Eng.*, 1992, **14**, (3), pp. 229–234

46 Ng, V.T., Lee, T.K.: 'Measuring border irregularities of skin lesions using fractal dimensions'. Photonics China '96, Int. Society for Optics and Photonics, 1996

47 Kikuchi, A., Kozuma, S., Sakamaki, K., *et al.*: 'Fractal tumor growth of ovarian cancer: sonographic evaluation', *Gynecol. Oncol.*, 2002, **87**, (3), pp. 295–302

48 Lee, T.K., McLean, D.I., Atkins, M.S.: 'Irregularity index: a new border irregularity measure for cutaneous melanocytic lesions', *Med. Image Anal.*, 2003, **7**, (1), pp. 47–64

49 Argenziano, G., Soyer, H.P., De Giorgio, V., *et al.*: 'Interactive atlas of dermoscopy (book and CD-ROM)' (EDRA Medical Publishing and New Media, 2000)

50 Iyatomi, H., Oka, H., Celebi, M.E.: 'An improved internet-based melanoma screening system with dermatologist-like tumor area extraction algorithm', *Comput. Med. Imaging Graph*, 2008, **32**, (7), pp. 566–579